Supporting Information

Turney *et al.* 10.1073/pnas.0801360105

SI Dating Methods and Results

Radiocarbon Dating and Stable Isotopic Analysis. The collagen was prepared in two ways for radiocarbon dating. Collagen extraction and step combustion (C-SC) followed a modified version of Longin's method (1). The bones were washed thoroughly in distilled water to remove all surface contamination. The sample was then broken into small pieces and decalcified by using dilute HCl. The insoluble residues were removed to isolate the gelatin, which was loaded into an ultralow-background ^{14}C vacuum line at the University of Wollongong and step-combusted to remove any labile contaminants. The carbon dioxide evolved at 850°C was collected, purified, and graphitized before measurement by AMS using the 14UD tandem accelerator in the Department of Nuclear Physics at the Australian National University (laboratory code ANUA-).

Collagen isolation using ultrafiltration (C-AF) followed that reported by Higham *et al.* (2). Coarsely ground bone powder (approximately 0.5–1 g) was loaded into a continuous-flow cell. An automated sequence of acid, base, and acid flowed through the cell over a period of 8 h, rinsing with ultrapure (MilliQ) water between each reagent. The crude collagen was gelatinized in a solution of pH 3 at 75°C for 20 h. Once complete, the gelatin solution was filtered by using a 8-μm polyethylene Eezi-filter, and insoluble residues were discarded. The filtered gelatin was then pipetted into the ultrafilter and centrifuged at 1,000–1,500 $\times g$ until 0.5–1 ml of the >30-kDa gelatin fraction remained. The remaining gelatin was freeze-dried ready for combustion in a CHN analyzer. Samples were measured for radiocarbon by AMS at the University of Oxford (laboratory code OxA-). Bone background samples were >60, >61, >54.6, >55.5, and >53.6 ka BP, indicating that measurements obtained were finite (Table S1).

For the stable isotopic analysis, between 1 and 5 mg of sample was weighed into tin capsules for automated combustion in an elemental analyzer interfaced to a continuous-flow isotope ratio mass spectrometer at Australian National University (extracted gelatin) and Queen's University Belfast (Lake Selina). Lake Selina (41°53′S, 145°36′E; 516 masl) bulk sediment samples were pretreated with 10% HCl to remove carbonates before measurement. The carbon dioxide gas evolved was resolved by using chromatographic separation on a GC column and analyzed for isotopic abundance. Standards and blanks were included during the run for internal calibration. $\delta^{13}C$ values are reported as per mille (‰) relative to PDB. Analytical precision for $\delta^{13}C$ at the 1 SD level is reported as 0.15‰. Radiocarbon ages were calibrated with OxCal by using the revised radiocarbon comparison curve from Cariaco Basin linked to the uranium-series dated Hulu Cave (3).

Optically Stimulated Luminescence (OSL) Dating. OSL dating provides an estimate of the time elapsed since luminescent minerals, such as quartz, were last exposed to sunlight (4–7). Buried grains will accumulate the effects of the nuclear radiation flux to which they are exposed, and the burial dose ["equivalent dose" (D_e)] can be measured by using the OSL signal. Measurements on quartz were made in the luminescence-dating laboratory at the University of Wollongong, and the burial ages were calculated from the equivalent dose divided by the total dose rate caused by ionizing radiation (Tables S2 and S3).

Sample Collection and Preparation. Lumps of dry sediment associated with megafaunal remains in museum collections were obtained for Scotchtown, Un-named, and Pleisto Scene Caves. The portion of each lump that had been exposed to light was removed in the laboratory under dim red illumination and retained for dose-rate determination. For the Mount Cripps sample, sediment grains trapped inside the nasal cavity of a *Protemnodon anak* skull (specimen GFV 5) were hand-picked in the luminescence-dating laboratory, after the removal of grains that would likely have been exposed to light after excavation of the skull; the latter material was used to estimate the dose rate. The remaining, light-safe, quartz grains of 90- to 250-μm diameter were isolated for OSL dating and purified by using standard procedures, including etching by hydrofluoric acid to remove the external α-dosed layer (5).

Equivalent Dose Determination. Equivalent doses were estimated from multigrain aliquots (≈80 grains per aliquot) of the Scotchtown, Un-named, and Pleisto Scene Cave samples, and 900 individual grains of the Mount Cripps sample were measured. In all instances, OSL data were obtained and analyzed by using the single-aliquot regenerative-dose (SAR) protocol, experimental apparatus, and statistical models described elsewhere (8–11).

Multigrain aliquots were stimulated by using blue (470 ± 30 nm) or green-plus-blue (420–550 nm) light for 100 s at 125°C, whereas single grains were stimulated by using a focused 10-mW green (532 nm) laser for 1 s at 125°C. In both cases, the natural and regenerative doses were preheated at 240°C for 10 s, and the test doses (which are used to correct for any sensitivity changes) were cut-heated to 160°C, before optical stimulation. Any malign effects arising from contamination of the quartz grains by infrared-sensitive inclusions (e.g., feldspars) were minimized in the multigrain aliquots by using an infrared (IR) bleach before blue- and/or green-light stimulation (10). For the single grains, the OSL IR depletion-ratio test (12) was conducted at the end of the measurement sequence to identify and reject any quartz grains found to be sensitive to IR stimulation (i.e., depletion ratios significantly smaller than unity). The ultraviolet OSL emissions were detected by using an Electron Tubes 9235QA photomultiplier tube fitted with a 7.5-mm Hoya U-340 filter, and laboratory doses were given by using a calibrated $^{90}Sr/^{90}Y$ β source.

Multigrain equivalent doses were determined from the first 3.2 s of OSL, and using the final 32 s as background, whereas single-grain equivalent doses were obtained from the first 0.11 s of signal, and using the final 0.17 s of OSL as background. The background-corrected counts were estimated by using Eq. 7 in ref. 13, and an instrumental reproducibility uncertainty of 2% was added (in quadrature) to each OSL measurement error for single grains (14). Dose-response curves were fitted by using a saturating exponential plus linear function, with the standard error on the equivalent dose determined by Monte Carlo simulation (15).

Routine checks of SAR protocol performance were made for thermal transfer, test-dose sensitivity correction, and dose-response behavior (14). Multigrain aliquots and single grains were rejected if they had thermally transferred signals >5% of the natural OSL at zero applied dose; "recycling ratios" (i.e., the reproducibility of a duplicate dose point) outside the range 0.9–1.1 for multigrain aliquots, or significantly different from unity for single grains; and dose-response curves that were saturated or did not intercept the natural OSL signal. Single grains were also rejected if their test-dose OSL signals (measured after stimulation of the natural OSL) were statistically indistinguishable from background. Under these same experimental and analytical conditions, correct dose estimates were obtained for multigrain aliquots of quartz from Mount Cripps, Scotchtown, and Un-named Cave that had been bleached before any measurements and then given a known dose. These samples gave ratios of measured/given dose of 1.002 ± 0.037 (n = 3), 1.012 ± 0.008 (n = 12), and 1.014 ± 0.010 (n = 6), respectively.

We used the central age model (8) to determine the relative spread ("overdispersion," σ_b) in equivalent dose remaining after making allowance for measurement uncertainties (16). The overdispersion estimates of 13 ± 3 and $16 \pm 4\%$ for the Scotchtown and Un-named Cave samples (Table S2) fall within the range of values (0–18%) reported for other multigrain aliquots of quartz that had been well bleached at deposition (16–19). Accordingly, the burial doses and OSL ages for the Scotchtown and Un-named Cave samples were calculated from the weighted mean of the 12 and 10 independent estimates of equivalent dose, respectively. The central age model was used to determine the weighted mean and its standard error because it takes into account the measured overdispersion.

For the Pleisto Scene Cave samples, however, many of the aliquots had natural OSL signals that were in dose saturation or that did not intercept the dose-response curve, so only minimum (infinite) equivalent doses could be obtained. The finite equivalent dose estimates for the few remaining aliquots are overdispersed by ≈30%, which is higher than typical values for well bleached quartz. Some of this additional overdispersion could be caused by the presence on each multigrain aliquot of dose-saturated grains, which will contribute significantly to the natural OSL signals but not to the regenerated OSL signals at high doses. The least-affected aliquots will be those that return the smallest equivalent doses, so we used the three-parameter minimum age model (8) to estimate the smallest equivalent dose for both Pleisto Scene Cave samples. This model takes into account the measurement uncertainty associated with each dose estimate, and, before running the model, we added (in quadrature) a value of 15% to each measurement error to represent the dose overdispersion present at deposition (16). Following ref. 20, we conservatively view the results as providing minimum estimates of burial dose and OSL age to allow for any bias caused by small equivalent doses being obtained from multigrain aliquots containing grains that have experienced below-average β dose rates, as can occur in limestone cave deposits (21).

Finite equivalent doses could be estimated for only 69 of the 900 grains analyzed from the Mount Cripps sample. The equivalent doses for these 69 grains range from 1.6 ± 0.4 to 157 ± 17 Gy and are overdispersed by $87 \pm 8\%$. We attribute this large overdispersion to two probable causes. First, it is unlikely that we successfully removed every grain that had been exposed to light in the nasal cavity of the skull since it was excavated, so the smallest equivalent doses may correspond to these postdepositionally bleached grains. Second, some of the 69 grains would likely have been situated next to, or encased by, carbonates derived from the limestone bedrock. These grains would have experienced greatly reduced β dose rates (21, 22), giving rise to smaller equivalent doses than those obtained for the majority of grains surrounded by noncarbonate materials.

We applied the finite mixture model (9, 23–25) to the 69 single-grain estimates of equivalent dose to identify the number of dose components (k), their corresponding equivalent doses and uncertainties, and the proportion of grains in each component. This model requires a user-defined estimate of the dose overdispersion for a sample of well bleached quartz grains, so we used values of 10–22% to cover the range of values reported in other single-grain studies (9, 10, 12, 14, 24). The optimal fit (as indicated by the smallest value for the Bayes Information Criterion) was achieved for a mixture of three dose components, each with an overdispersion value of 18%; our general conclusions, however, are insensitive to the particular value chosen. Table S3 lists the corresponding equivalent dose and age estimates and the relative proportion of each component. The equivalent doses for 64 of these grains (which constitute the two main components, $k2$ and $k3$) are plotted in Fig. S1, whereas the values of <10 Gy obtained for the remaining 5 grains (which comprise component $k1$) have been omitted for clarity of presentation.

We consider the equivalent dose of component $k3$ (which contains the majority of grains) to correspond most closely to the time of deposition of grains in the skull (36 ± 3 ka). Postdepositional light exposure of the 5 grains in component $k1$ likely accounts for its low equivalent dose and age. For component $k2$, the single-grain equivalent doses are consistent with those expected for grains located next to, or encased by, carbonates; such grains would have experienced β dose rates much lower than the average β dose rate for the bulk sample, which is used to calculate the OSL age. Reducing the β dose rate for the bulk sample to zero (as a first approximation of the radiation field affecting a grain surrounded entirely by carbonate) increases the age of component $k2$ from 13.2 ± 1.4 ka (Table S3) to 30 ± 3 ka, which is not significantly different from the age of component $k3$.

Dose-Rate Determination. The total dose rate for each sample was calculated as the sum of the β and γ dose rates attributable to radioactive decay of ^{238}U, ^{235}U, ^{232}Th (and their daughter products) and ^{40}K. Account was also taken of the cosmic-ray contribution [adjusted for site altitude, geomagnetic latitude, and thickness of rock and sediment overburden (26)] and the effective α dose rate from radioactive inclusions internal to the quartz grains [estimated from measurements made previously on quartz grains from southeastern Australia (27)]. For the Scotchtown, Un-named, and Pleisto Scene Cave samples, ≈40 g of the light-exposed material removed during sample preparation was measured by high-resolution γ-ray spectrometry (21, 28), and the radionuclide activities were converted to dose rates (29). Less material was available for the Mount Cripps sample, so we used a combination of thick-source α counting (TSAC) to determine the U and Th concentrations and β counting to measure directly the total β dose rate from U, Th, and K (30). The γ dose rate was calculated from the individual U, Th, and K concentrations, the last deduced from the difference between the β dose rates obtained by TSAC and β counting. In all cases, allowance was made for β dose attenuation (31) and sample water content (30).

The sediment samples were obtained from museum collections, where they had been allowed to dry. We therefore have no direct measure of the field water contents, and we have adjusted the dry β and γ dose rates for an assumed field water content of $15 \pm 5\%$. At the 95% confidence interval, values of between 5 and 25% encompass most of the present-day field water contents measured for OSL dating of other cave deposits across temperate southern Australia (19, 32), and this range also allows for substantial long-term variations in water content. As an indication of the effect of water content variation on the calculated OSL age, each 1% increase in water content generates an age increase of ≈1%.

The high-resolution γ spectrometry data (Table S2) show that a condition of secular equilibrium currently exists in the ^{232}Th decay series of samples from Scotchtown and Un-named Cave and also sample MU203–205 from Pleisto Scene Cave, as is commonly the case for Australian terrestrial sediments (21, 28). The small extent of apparent disequilibrium between ^{228}Ra and ^{228}Th in sample MU206 from Pleisto Scene Cave has a negligible effect on the dose rate. The weighted mean of the ^{228}Ra and ^{228}Th activities was used in the calculations of total dose rate and OSL age for each of these four samples.

In the ^{238}U decay series, there is significant disequilibrium between ^{226}Ra and ^{210}Pb for all four samples (Table S2). The $^{210}Pb/^{226}Ra$ ratios are consistent with 22–53% escape of radon (^{222}Rn) gas to the atmosphere. Such high radon losses have been reported previously for cave sediments on the Nullarbor Plain (20, 21), and we have assumed that the measured ratios persisted throughout the period of sample burial. If, however, all of the radon loss resulted from sediment disturbance during excavation of the fossils and associated deposits, and the ^{226}Ra activities are used to represent the ^{210}Pb values, then the calculated ages for samples ST1, JF155, MU203–205 and MU206 decrease to 52 ± 4, 99 ± 9, >101 ± 22, and >96 ± 16 ka, respectively. These are consistent at the 68% confidence interval (or the 95% confidence interval for sample MU206) with the ages shown in Table S2. There is also evidence of disequilibrium between ^{238}U and ^{226}Ra in these four samples. MU203–205 is the only sample that contained no bone fragments, and we attribute the ^{238}U deficit (of ≈16%) to uranium leaching in association with carbonate complexes. The other samples have an excess of ^{238}U (of 3–28%), which we attribute to the absorption of uranium by the disseminated bone fragments after burial. However, uranium disequilibria of such magnitude have a negligible effect on the total dose rate (21, 28), so the measured radionuclide activities were used to calculate the OSL ages.

The equilibrium status of the Mount Cripps sample cannot be assessed from the TSAC and β-counting measurements, but any U-series disequilibria will have a minor effect on the calculated age of this sample when using such techniques (21, 28) because the ^{238}U decay chain accounts for only ≈22% of the total dose rate. As with the other four samples, therefore, the OSL age was calculated under the assumption that the present-day dose rate prevailed throughout the period of sample burial. The OSL age of 36 ± 3 ka (Table S3) for sediments trapped in the nasal cavity of the *P. anak* skull is slightly younger than the most reliable ^{14}C ages for the same specimen (41.8–40.9 ka, obtained from gelatin isolated by ultrafiltration), with all ages expressed at the 68% confidence interval. This result is compatible with the postmortem intrusion of sediment grains into the skull soon after burial.

Lake Selina. The record from the Lake Selina sequence spans the last glacial–interglacial cycle (33). Because the original chronology is considered relatively imprecise, the vegetation record was matched against the orbitally-dated $\delta^{18}O$ marine record of Martinson *et al*. (34).

1. Longin R (1971) New method of collagen extraction for radiocarbon dating. *Nature* 230:241–242.
2. Higham TFG, Jacobi RM, Ramsey CB (2006) AMS radiocarbon dating of ancient bone using ultrafiltration. *Radiocarbon* 48:179–195.
3. Hughen K, Southon J, Lehman S, Bertrand C, Turnbull J (2006) Marine-derived ^{14}C calibration and activity record for the past 50,000 years updated from the Cariaco Basin. *Quat Sci Rev* 25:3216–3227.
4. Huntley DJ, Godfrey-Smith DI, Thewalt MLW (1985) Optical dating of sediments. *Nature* 313:105–107.
5. Aitken MJ (1998) *An Introduction to Optical Dating* (Oxford Univ Press, Oxford, UK).
6. Bøtter-Jensen L, McKeever SWS, Wintle AG (2003) *Optically Stimulated Luminescence Dosimetry* (Elsevier, Amsterdam).
7. Lian OB, Roberts RG (2006) Dating the Quaternary: Progress in luminescence dating of sediments. *Quat Sci Rev* 25:2449–2468.
8. Galbraith RF, Roberts RG, Laslett GM, Yoshida H, Olley JM (1999) Optical dating of single and multiple grains of quartz from Jinmium rock shelter, northern Australia. I. Experimental design and statistical models. *Archaeometry* 41:339–364.
9. Roberts RG, Galbraith RF, Yoshida H, Laslett GM, Olley JM (2000) Distinguishing dose populations in sediment mixtures: a test of single-grain optical dating procedures using mixtures of laboratory-dosed quartz. *Radiat Meas* 32:459–465.
10. Olley JM, Pietsch T, Roberts RG (2004) Optical dating of Holocene sediments from a variety of geomorphic settings using single grains of quartz. *Geomorphology* 60:337–358.
11. Wintle AG, Murray AS (2006) A review of quartz optically stimulated luminescence characteristics and their relevance in single-aliquot regeneration dating protocols. *Radiat Meas* 41:369–391.
12. Jacobs Z, Duller GAT, Wintle AG (2003) Optical dating of dune sand from Blombos Cave, South Africa. II. Single grain data. *J Hum Evol* 44:613–625.
13. Galbraith R (2002) A note on the variance of a background-corrected OSL count. *Ancient TL* 20:49–51.
14. Jacobs Z, Duller GAT, Wintle AG (2006) Interpretation of single-grain D_e distributions and calculation of D_e. *Radiat Meas* 41:264–277.
15. Yoshida H, Roberts RG, Olley JM (2003) Progress towards single-grain optical dating of fossil mud-wasp nests and associated rock art in northern Australia. *Quat Sci Rev* 22:1273–1278.
16. Galbraith RF, Roberts RG, Yoshida H (2005) Error variation in OSL palaeodose estimates from single aliquots of quartz: A factorial experiment. *Radiat Meas* 39:289–307.
17. Jacobs Z, Wintle AG, Duller GAT (2003) Optical dating of dune sand from Blombos Cave, South Africa. I. Multiple grain data. *J Hum Evol* 44:599–612.
18. Anderson A, *et al.* (2006) Times of sand: Sedimentary history and archaeology at the Sigatoka Dunes, Fiji. *Geoarchaeology* 21:131–154.
19. Prideaux GJ, *et al.* (2007) Mammalian responses to Pleistocene climate change in southeastern Australia. *Geology* 35:33–36.
20. Prideaux GJ, *et al.* (2007) An arid-adapted middle Pleistocene vertebrate fauna from south-central Australia. *Nature* 445:422–425.
21. Olley JM, Roberts RG, Murray AS (1997) Disequilibria in the uranium decay series in sedimentary deposits at Allen's Cave, Nullarbor Plain, Australia: Implications for dose-rate determinations. *Radiat Meas* 27:433–443.
22. Jacobs Z, Wintle AG, Roberts RG, Duller GAT (2008) Equivalent dose distributions from single grains of quartz at Sibudu, South Africa: Context, causes and consequences for optical dating of archaeological deposits. *J Arch Sci* 35:1808–1820.
23. David B, *et al.* (2007) Sediment mixing at Nonda Rock: Investigations of stratigraphic integrity at an early archaeological site in northern Australia and implications for the human colonisation of the continent. *J Quat Sci* 22:449–479.
24. Jacobs Z, Wintle AG, Duller GAT, Roberts RG, Wadley L (2008) New ages for the post-Howiesons Poort, late and final Middle Stone Age at Sibudu, South Africa. *J Arch Sci* 35:1790–1807.
25. Jacobs Z, Roberts RG (2007) Advances in optically stimulated luminescence dating of individual grains of quartz from archeological deposits. *Evol Anthrop* 16:210–223.
26. Prescott JR, Hutton JT (1994) Cosmic ray contributions to dose rates for luminescence and ESR dating: Large depths and long-term time variations. *Radiat Meas* 23:497–500.
27. Bowler JM, *et al.* (2003) New ages for human occupation and climatic change at Lake Mungo, Australia. *Nature* 421:837–840.
28. Olley JM, Murray A, Roberts RG (1996) The effects of disequilibria in the uranium and thorium decay chains on burial dose rates in fluvial sediments. *Quat Sci Rev* 15:751–760.
29. Stokes S, *et al.* (2003) Alternative chronologies for Late Quaternary (Last Interglacial–Holocene) deep-sea sediments via optical dating of silt-sized quartz. *Quat Sci Rev* 22:925–941.
30. Aitken MJ (1985) *Thermoluminescence Dating* (Academic, London).
31. Mejdahl V (1979) Thermoluminescence dating: Beta-dose attenuation in quartz grains. *Archaeometry* 21:61–72.
32. Roberts RG, *et al.* (2001) New ages for the last Australian megafauna: Continent-wide extinction about 46,000 years ago. *Science* 292:1888–1892.
33. Colhoun EA, Pola JS, Barton CE, Heijnis H (1999) Late Pleistocene vegetation and climate history of Lake Selina, western Tasmania. *Quat Int* 57/58:5–23.
34. Martinson DG, *et al.* (1987) Age dating and the orbital theory of the Ice Ages: Development of a high-resolution 0 to 300,000-year chronostratigraphy. *Quat Res* 27:1–29.
35. Goede A, Bada JL (1985) Electron spin resonance dating of Quaternary bone material from Tasmanian caves: A comparison with ages determined by aspartic acid racemization and ^{14}C. *Aust J Earth Sci* 32:155–162.
36. Prideaux GJ (2004) *Systematics and Evolution of the Sthenurine Kangaroos* (Univ Calif Publ Geol Sci No. 146).
37. Gill ED, Banks MR (1956) Cainozoic history of Mowbray Swamp and other areas of northwestern Tasmania. *Rec Queen Vic Mus* (*Launceston*) 6:1–42.
38. Banks MR, Colhoun EA, van De Geer G (1976) Late Quaternary *Palorchestes azael* (Mammalia, Diprotodontidae) from northwestern Tasmania. *Alcheringa* 1:159–166.
39. Goede A, Murray P (1977) Pleistocene man in south central Tasmania: Evidence from a cave site in the Florentine Valley. *Mankind* 11:2–10.

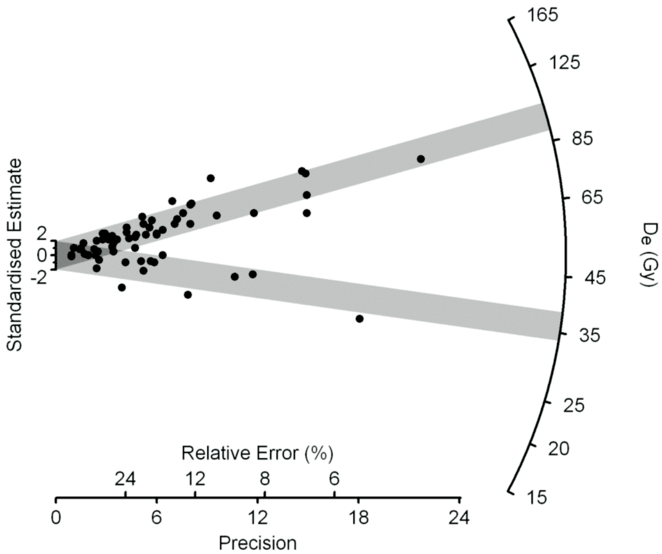

Fig. S1. Equivalent dose estimates from Mount Cripps. Radial plot (8) of the equivalent dose (D_e) estimates obtained from 64 (of 69) individual grains of quartz from the Mount Cripps sample; the other five measured values (all smaller than 10 Gy) form a separate dose component (*k*1) and have been omitted for clarity. The equivalent dose for a grain is read by drawing a line from the origin of the *y* axis (Standardized Estimate) through the data point of interest, until the line intersects the radial axis (log scale) on the right side. The measurement error on this equivalent dose is obtained by extending a line vertically to intersect the *x* axis. The latter has two scales: the relative standard error and its reciprocal (Precision). Hence, the most precise estimates fall furthest to the right of the plot, and the least precise estimates fall furthest to the left. If the equivalent doses are statistically consistent with a common dose (i.e., the spread in values is caused solely by measurement error), then 95% of the data points should be captured by a band ±2 units in width projecting from the standardized estimate axis. By using the finite mixture model (9), the plotted data can be resolved into two dose components (each shown by a shaded band): a dominant component (*k*3, containing ≈71% of grains) centered at ≈97 Gy, and a secondary component (*k*2, consisting of ≈22% of grains) centered at ≈36 Gy. We attribute the latter component to the reduced β dose rate experienced by individual grains located next to, or surrounded by, carbonates, and component *k*1 (not shown) to incomplete removal during sample preparation of postdepositionally bleached grains. Component *k*3 provides the most accurate estimate of burial age when, as here, it is determined from the equivalent dose divided by the total dose rate for the bulk sample.

Table S1. Radiocarbon ages

Site	Sample	Laboratory code	Preparation method	$\delta^{13}C$, ‰	C:N ratio	Collagen (%)	^{14}C age ± 1 SD (yr BP)	Calibrated 1 SD ^{14}C age range (ka)
Mount Cripps	*Protemnodon* cf. *anak* (QVM:2001:GFV 2a)	OxA-16417	C-AF	−23.1	3.2	10.5	36,200 ± 300	41.8–40.9
Mount Cripps	*Protemnodon* cf. *anak* (QVM:2001:GFV 2a)	ANUA-33018	C-SC	−22.2	3.2	6.6*	32,780 ± 370	38.0–36.3
Mount Cripps	*Protemnodon* cf. *anak* (QVM:2001:GFV 2b)	OxA-16418	C-AF	−23.7	3.2	10.5	37,920 ± 340	42.9–42.1
Mount Cripps	*Protemnodon* cf. *anak* (QVM:2001:GFV 2b)	ANUA-34216/ ANUA-34217	C-SC	−23.0	2.8	5.1*	30,400 ± 270	35.0–34.4
Titans Shelter	*Protemnodon* cf. *anak* (Z3370)	ANUA-31230	C-SC	−24.3	2.8	3.5	39,980 ± 610	44.9–43.0

C-SC denotes collagen-stepped combustion (University of Wollongong/Australian National University). C-AF denotes collagen-ultrafiltration (Oxford University). Samples were also collected from Site M Beginner's Luck Cave JF-79 (Z3371 *Simosthenurus* sp. femur), Pleisto Scene Cave MU206 (Z3372 *Simosthenurus* sp. pelvis), Pleisto Scene Cave MU206 (Z3373 *Macropodine* sp. humerus), and Scotchtown; unfortunately, insufficient collagen could be extracted from these samples for radiocarbon dating.

*Salt contamination of the C-SC samples necessitated several filtrations, which may have led to relatively low collagen yields.

Table S2. Dose-rate data, equivalent doses, and OSL ages for sediment samples from Scotchtown, Un-named, and Pleisto Scene Caves

Sample code	Grain diameter, μm	Radionuclide activities,* Bq kg^{-1}						Cosmic-ray dose rate,† Gy ka^{-1}	Total dose rate‡§, Gy ka^{-1}	Equivalent dose‡¶, Gy	No. of aliquots/ σ_b‖, %	OSL age‡, ka
		^{238}U	^{226}Ra	^{210}Pb	^{228}Ra	^{228}Th	^{40}K					
Scotchtown Cave												
ST1	90–125	33.5 ± 0.9	29.8 ± 0.3	15.9 ± 0.9	22.9 ± 0.5	21.9 ± 0.3	485 ± 9	0.17	2.20 ± 0.13	123 ± 5 (C)	12/ 13 ± 3	56 ± 4
Un-named Cave												
JF155	90–125	19.0 ± 0.8	14.9 ± 0.2	11.6 ± 0.7	18.5 ± 0.4	18.7 ± 0.3	149 ± 5	0.15	1.09 ± 0.07	112 ± 7 (C)	10 / 16 ± 4	103 ± 9
Pleisto Scene Cave												
MU203–205	90–125	47.8 ± 1.3	57.2 ± 0.4	26.7 ± 1.3	36.4 ± 0.7	35.1 ± 0.5	110 ± 4	0.13	1.50 ± 0.09	>191 ± 40 (M)	4/ 30 ± 11	>127 ± 28
MU206	90–125	43.2 ± 1.1	41.8 ± 0.3	20.8 ± 1.1	19.5 ± 0.5	17.5 ± 0.3	63.1 ± 2.4	0.13	1.02 ± 0.07	>123 ± 19 M)	5 / 31 ± 10	>120 ± 21

*Measurements made on ≈40 g of dried, homogenized, and powdered sample by high-resolution γ-ray spectrometry. The samples were stored dry in museum collections, so their field water contents are unknown. The dry dose rates calculated from the radionuclide activities have, therefore, been adjusted for an assumed field water content of 15 ± 5% (expressed as percentage of dry mass of sample), which encompasses (at the 95% confidence interval) the typical range of values measured for other cave sediments in temperate southern Australia (19, 32). The OSL ages increase by ≈1% for each 1% increase in water content.

†Assigned relative uncertainty of ±20%.

‡Mean ± total uncertainty (68% confidence interval), calculated as the quadratic sum of the random and systematic uncertainties.

§Includes assumed internal α dose rate of 0.03 ± 0.01 Gy ka^{-1}.

¶Estimated using the central (C) or three-parameter minimum (M) age model (8). An overdispersion (σ_b) value of 15% was added in quadrature to the measurement error for each aliquot before running the minimum age model (16). The total uncertainty includes a systematic component of ±2% associated with laboratory β source calibration.

‖No. of aliquots used for equivalent dose determination/overdispersion (σ_b), the relative standard deviation of the equivalent dose distribution after allowing for measurement uncertainties (16).

Table S3. Dose rate data, equivalent doses and OSL ages for sediment sample from Mount Cripps

Sample code	Grain diameter, μm	Radionuclide concentrations*			Dose rates,* Gy ka^{-1}		Total dose rate,†‡ Gy ka^{-1}		Equivalent dose,§ Gy	Proportion of grains,§ %	OSL age,† ka
		U, μg g^{-1}	Th, μg g^{-1}	K, %	β	γ					
MC1	90–250	2.93 ± 0.36	10.30 ± 1.17	1.69 ± 0.09	1.53 ± 0.12	1.05 ± 0.08	2.72 ± 0.20	*k*1	4.2 ± 0.5	7 ± 3	1.5 ± 0.2
								*k*2	35.8 ± 2.6	22 ± 6	13.2 ± 1.4
								***k*3**	**96.7 ± 4.0**	**71 ± 6**	**36 ± 3**

*Measurements made on a dried, homogenized, and powdered sample by thick-source α counting for separate U and Th concentrations and by β counting for combined dose rate due to U, Th, and K; the K concentration was obtained from the difference. The γ dose rate was calculated from the individual U, Th, and K concentrations, whereas the β dose rate was estimated directly from the β-counting measurements. As with the other samples dated in this study, dry dose rates were adjusted for an assumed field water content of 15 ± 5% (see Table S2, first footnote).

†Mean ± total uncertainty (68% confidence interval), calculated as the quadratic sum of the random and systematic uncertainties.

‡Includes cosmic-ray dose rate of 0.11 ± 0.02 Gy ka^{-1} and an assumed internal α dose rate of 0.03 ± 0.01 Gy ka^{-1}.

§Mean ± SE, estimated for 69 single grains using the finite-mixture model (9). Three dose components (*k*1–3) were identified with the overdispersion (σ_b) value set at 18%. Equivalent-dose component *k*3 (shown in bold type) contains the highest proportion of grains and is considered the most reliable indicator of sample burial age. A systematic uncertainty of ±2% associated with laboratory β source calibration was added in quadrature to the SE before age determination.

Table S4. Tasmanian sites with megafauna assemblages

1) Mount Cripps chamber CP213 (41°37′S, 145°46′; 355 masl) (^{14}C: 37.9–36.2 ka BP; OSL: 36 ± 3 ka)

Protemnodon cf. *anak*
QVM:2001:GFV 5 (and associated remains) Cranium of large subadult with P3 and M4 unerupted, lacking zygomata and with damage to nasals and cranial vault. Right pelvis; left femur; right fibula; three distal and one proximal thoracic vertebrae; first and second lumbar vertebrae, first and second caudal vertebrae, and a more distal caudal.

QVM:2000:GFV 10 (and associated remains) Well preserved cranium with P3, M2–4 unerupted, lacking premaxillae; right dentary with lower incisor; right humerus and ulna, left and right tibia.

QVM:2001:GFV 9 Right maxilla with M1 erupting, left and right dentaries with incisors; two proximal caudal vertebrae; left humerus and right ulna; left and right ischia; left and right femurs; left and right tibias. Mass ≈30 kg.

Also
Thylogale billardierii
Potorous tridactylus
Trichosurus vulpecula
Pseudocheirus peregrinus
Vombatus ursinus
Antechinus swainsonii
Dasyurus viverrinus
Dasyurus maculatus
Sarcophilus harrisii
Mastacomys fuscus
Pseudomys higginsi
Rattus lutreolus

2) Mount Cripps, chamber CP118 (41°37′S, 145°46′; 355 masl) (undated)

Metasthenurus newtonae

3) Titans Shelter site G (42°35′S, 146°28′; 400 masl) (^{14}C: 40 ka BP; ESR: 27 ka; AAR: 40 ka) (35)

?*Zygomaturus* sp.
Protemnodon sp.
Macropus giganteus titan
Macropus rufogriseus
Simosthenurus occidentalis (36)
Macropus rufogriseus
Thylogale billardierii
Sarcophilus harrisii
Dasuyrus viverrinus
Pseudocheirus peregrinus
Vombatus ursinus
Mastacomys fuscus

4) Mowbray Swamp (^{14}C: >37.8 ka BP) (37)

Zygomaturus trilobus
Palorchestes azael
Macropus giganteus titan
Macropus greyi

5) Main Cave, near Montagu (35)

Simosthenurus occidentalis (36)

6) Pulbeena Limeworks (^{14}C: >54.2 ka BP) (38)

Palorchestes azael

7) Scotchtown Cave (40°53′S, 145°06′; 30 masl) (OSL: 56 ± 4 ka) (37).

Megalibgwilia sp.
Metasthenurus newtonae (36)
Palorchestes azael
Zygomaturus trilobus
Thylacoleo carnifex
Simosthenurus occidentalis
Protemnodon cf. *anak*
Thylacinus cynocephalus
Sarcophilus harrisii
Macropus giganteus titan
Macropus rufogriseus
Thylogale billardierii
Potorous tridactylus
Trichosurus vulpecular
Vombatus ursinus
Mastacomys fuscus

8) Beginner's Luck Cave, Site M (JF-79) Florentine Valley (ESR: 63 ka; AAR: 80 ka) (35, 39). *S. occidentalis* comes from site M in cave, which is a surface scatter of bones only (39).

Thylacoleo sp. (distal ulna)
Macropus giganteus (calcaneum)
Simosthenurus occidentalis (36)

9) Un-named Cave (JF-155, Florentine Valley; 42°32′S, 146°27′; 400 masl) (OSL: 103 ± 9 ka; ESR: 97 ka; AAR: 30 ka) (35). On archived bag of bones (a) "small shelter on breccia ridge, Settlement Rd, Florentine Valley 21 XI 1976".

Protemnodon sp. (5th mtt)
Macropus giganteus (proximal tibia)
Macropus rufogriseus
Thylacoleo sp. P3
Simosthenurus sp. (4th mtt)

10) Pleisto Scene Cave (MU203–205 and MU206; 40°51′S, 144°54′; 20–40 masl) (OSL: >127 ± 28 ka and >120 ± 21 ka; ESR: 310 ka; AAR: 130 ka and 110 ka) (35).

Megalibgwilia sp.
Sarcophilus harrisii
Perameles gunnii
Vombatus ursinus
Thylacoleo sp.
Potorous tridactylus
Thylogale billardierii
Protemnodon cf. *anak*
Macropus rufogriseus
Macropus giganteus
Simosthenurus occidentalis (36)
? *Zygomaturus*
Palorchestes sp.
Mastacomys fuscus
Hydromys chrysogaster

^{14}C denotes radiocarbon age; OSL, optically stimulated luminescence; AAR, amino acid racemization; ESR, electron spin resonance.

Table S5. Dental measurements for *Protemnodon* cf. *anak*, Mount Cripps, Chamber 213

P2/	l	12.0, 12.0, 11.3
	aw	6.1, 6.1, 7.0
	pw	8.0, 7.6, 8.0
DP3/	l	11.1, 12.1, 11.4
	aw	9.5, 9.2, 9.4
	pw	9.5, 9.9, 10
M1/	l	13.0, 13.1, 12.9
	aw	10.9, 11.3, 10.5
	pw	10.6, 11.1, 10.5
M2/	l	14.3
	aw	12.0
	pw	11.6
M3/	l	15.1
	aw	12.9
	pw	11.8
M4/	l	15.0
	aw	12.9
	pw	11.0
P/2	l	11.4, 10.5
	aw	4.9, 5.3
	pw	6.0, 5.4
DP/3	l	11.0, 10.8
	aw	6.7, 6.1
	pw	7.4, 6.9
M/1	l	13.5, 13.1
	aw	8.5, 8.0
	pw	9.1, 8.9
Metasthenurus newtonae, Mount Cripps		
M/2	l	14.0
	aw	11.9
	pw	12.2
M/3	l	15.1
	aw	12.5
	pw	12.5
M/4	l	15.0
	aw	—
	pw	11.2

Length (l), anterior width (aw), and posterior width (pw) measurements given in mm.